Multichromophore Molecular Design for Thermally Activated Delayed Fluorescence Emitters with Near-Unity Photoluminescence Quantum Yields

Dongyang Chen,[a] Yu Kusakabe,[b] Yongxia Ren,[b] Dianming Sun,[a] Pachaiyappan Rajamalli,[a] Yoshimasa Wada,[b] Katsuaki Suzuki,[b] Hironori Kaji,[b] and Eli Zysman-Colman[a*]*

[a] Organic Semiconductor Centre, EaStCHEM School of Chemistry, University of St Andrews, St Andrews, Fife, UK, KY16 9ST, Fax: +44-1334 463808; Tel: +44-1334 463826; E-mail: eli.zysman-colman@st-andrews.ac.uk;
[b] Institute for Chemical Research, Kyoto University, Uji, Kyoto, 611-0011, Japan
E-mail: kaji@scl.kyoto-u.ac.jp

Abstract

Three multichromophore thermally activated delayed fluorescence (TADF) molecules, ***p*-di2CzPN**, ***m*-di2CzPN**, and **1,3,5-tri2CzPN**, were synthesized and characterized. These molecules were designed by connecting the TADF moiety 4,5-di(9*H*-carbazol-9-yl)phthalonitrile (**2CzPN**) to different positions of a central benzene ring scaffold. Three highly soluble emitters all exhibited near quantitative photoluminescence quantum yields (Φ_{PL}) in toluene. High Φ_{PL}s were also achieved in doped films, 59% and 70% for ***p*-di2CzPN** and ***m*-di2CzPN** in 10 wt% DPEPO doped films, respectively, and 54% for **1,3,5-tri2CzPN** in 20 wt% doped CBP film. The rate constant of reverse intersystem crossing (k_{RISC}) for ***p*-di2CzPN** and ***m*-di2CzPN** in DPEPO films reached 1.1×10^5 and 0.7×10^5 s^{-1}, respectively, and k_{RISC} for **1,3,5-tri2CzPN** in CBP film reached 1.7×10^5 s^{-1}. A solution-processed organic light-emitting diode based on **1,3,5-tri2CzPN** exhibited a sky-blue emission with CIE coordinate of (0.22, 0.44), and achieved a maximum external quantum efficiency of 7.1%.

Introduction

Given their huge potential in displays and solid-state lighting technologies, there remains continued strong interest in improving the performance of organic light-emitting diodes (OLEDs).[1–4] The emitters utilized in OLEDs dictate the performance and efficiency of the electroluminescent (EL) device. Over the years, researchers have explored different classes of emitters in OLEDs.[5–8] Fluorescence emitters were firstly employed to generate stable electroluminescence.[1,5,6] However, as these emitters cannot harvest the triplet excitons generated in the device, 75% of the excitons are lost as heat and the maximum internal quantum efficiency (IQE) is limited to 25%.[9] Phosphorescence emitters were developed to harness the triplet excitons and thereby improve the IQE of the device.[10] The spin-orbit coupling mediated by the heavy metal atoms in the organometallic complexes that act as emitters facilitate both intersystem crossing of singlet excitons to triplets and radiative decay from the lowest triplet excited state (T_1) to the ground state (S_0) as phosphorescence, making it possible to realize unity IQE.[10,11] Detracting features of organometallic phosphors include the unstable emission of blue emitters and the scarcity of the noble metals, which has prompted researchers to look for new materials classes.[11–13] The discovery that thermally activated delayed fluorescence (TADF) emitters can be effectively utilized in EL devices has brought about a breakthrough in the development of OLEDs.[14–16] In TADF molecules, triplet excitons can be thermally up-converted to singlet excitons via reverse intersystem crossing (RISC).[15–17] The excitons then decay radiatively to S_0 without the assistance of heavy metals.[15–17] The highly tunable emission, high photoluminescence (PL) quantum yields (Φ_{PL}), and ready availability of the compounds

at frequently low expense have earned TADF-based OLEDs the title of the third generation of OLEDs.[4] Efficient TADF emitters rely on a small singlet-triplet energy splitting (ΔE_{ST}) to achieve high RISC rates.[18–20] The molecular design is based on a small exchange integral between frontier molecular orbitals that is frequently obtained by separating and/or electronically decoupling the donor and acceptor fragments of the TADF molecule.[18–21] However, most TADF emitters exhibit low Φ_{PL} as the limited overlap between the highest occupied molecular orbital (HOMO) and lowest unoccupied molecular orbital (LUMO) also leads to a low oscillator strength (*f*), resulting in an inefficient radiative decay from lowest singlet excited state (S_1) to S_0.[22,23] Tremendous efforts have been devoted to designing molecules that achieve simultaneously small ΔE_{ST} and high Φ_{PL}.[24–27]

Increasing the oscillator strength will enhance the radiative decay and can lead to higher Φ_{PL}, considering the molecule as a classical oscillating dipole, the *f* value is proportional to the integral of absorption coefficients (ε) over entire the absorption band (equation 1):[28]

$$f = 4.3 \times 10^{-9} \int \varepsilon\,(v) dv \qquad (1)$$

Where ε is the absorption coefficient and v is the energy of the transition in wave numbers. Thus, the Φ_{PL} of TADF molecules can be increased by intensifying light absorption, which can occur by incorporating two luminophores into one emitter molecule.[29,30] Lee *et al.* firstly explored a dual emitting core design where two TADF luminophores were directly connected via a single bond.[29–31] The blue TADF emitter, 4,6-di(carbazol-9-yl)isophthalonitrile (DCzIPN) was utilized as the luminophore and dual cores emitters, named DDCzIPN, 33TCzPN, 34TCzPN, and 44TCzPN were obtained by connecting two DCzIPN molecules at different

positions (Figure **1**).[29,30] The common feature of these emitters is that ΔE_{ST} remains largely unaffected but the Φ_{PL} increases.[29,30] As a result, the maximum external quantum efficiency (EQE_{max}) of the OLEDs improved from 16.4% for DCzIPN to 18.9% (DDCzIPN), 17.4% (33TCzPN), 20.5% (34TCzPN), and 19.5% (44TCzPN).[29,30] Deep blue emission with narrowed full width at half-maximum (FWHM) was also achieved in CzBPCN, which contains dual TADF cores.[31] The carbazoles from the dual cores form an interlocked structure to suppress the rotation of the central biphenyl ring. The molecule exhibited deep blue emission with maximum wavelength of photoluminescence (λ_{PL}) at 453 nm and Φ_{PL} of 76% in toluene.[31] The OLED showed an EQE_{max} of 14.0% with a narrow FWHM of 48 nm leading to deep blue emission with CIE coordinates of (0.14, 0.12).[31] Lee *et al.* also reported the triazine- and carbazole-containing dual core emitter mCBPTrz-1.[32] This emitter exhibited ultra-high Φ_{PL} of 94% in DPEPO film compared to 17% for the reference emitter CzTrz, showing a slightly red-shifted PL spectrum in the film (λ_{PL} of 455 nm and 460 nm for CzTrz and mCBPTrz-1, respectively).[32] The OLED with mCBPTrz-1 exhibited over 20% EQE_{max} with maximum wavelength of electroluminescence (λ_{EL}) of 503 nm and CIE coordinates of (0.23, 0.52), which was double the efficiency compared to the device based on CzTrz.[32,33] This dual emitting strategy was adopted by other groups towards high-efficiency TADF emitter design. Yang *et al*. reported two TADF emitters bearing dual emitting cores 2,2′-DPXZ-PN and 3,3′-DPXZ-PN.[34] Compared to the mono emitter PXZ-PN, 2,2′-DPXZ-PN and 3,3′-DPXZ-PN showed increased molar absorptivity coefficients in toluene for the charge transfer (CT) state and the Φ_{PL} values also increased from 49% of PXZ-CN to 67% and 82%, respectively, for 2,2′-DPXZ-PN and 3,3′-DPXZ-PN in 10 wt% doped CBP films.[34] As a result, the devices with 2,2′-DPXZ-PN and 3,3′-

DPXZ-PN showed respective EQE_{max} of 13% and 15%, together with small efficiency roll-off (12% and 14% at 1000 cd m^{-2}, respectively).[34] Choi *et al.* reported a treble core TADF emitter IAcTr-out wherein diphenyltriazine acceptors were linked to three indenoacridine donors that are attached around a central benzene ring.[35] The IAcTr-out possessed a small ΔE_{ST} of 0.05 eV and Φ_{PL} of 48% in 25 wt% doped mCP film. The TADF emitter exhibited aggregation-induced emission (AIE) and the solution-processed OLED showed an EQE_{max} of 17.5% with CIE of (0.29, 0.54).[35] These examples demonstrate that the multiple emitting cores design is an effective approach to improve molecular photophysics and electroluminescence properties.[31–35]

In this work, we connect 4,5-di(9*H*-carbazol-9-yl) phthalonitrile (**2CzPN**) to a central benzene ring to construct dual and treble core TADF emitters and these emitters achieved both high Φ_{PL} and small ΔE_{ST}. The different connecting positions to a central benzene ring, namely 1,4 positions, 1,3 positions and 1,3,5 positions, offering three multichoromphore emitters: ***p*-di2CzPN**, ***m*-di2CzPN** and **1,3,5-tri2CzPN**, respectively. The Φ_{PL} values of these three emitters all reached 100% in toluene, and the k_{RISC} values reached 10^5 s^{-1} in small molecule host matrices. The three emitters also exhibited high solubility in most organic solvent, making it possible to fabricate solution-processed OLEDs. An initial version of this work was deposited in ChemRxiv on 08/05/2021.[36]

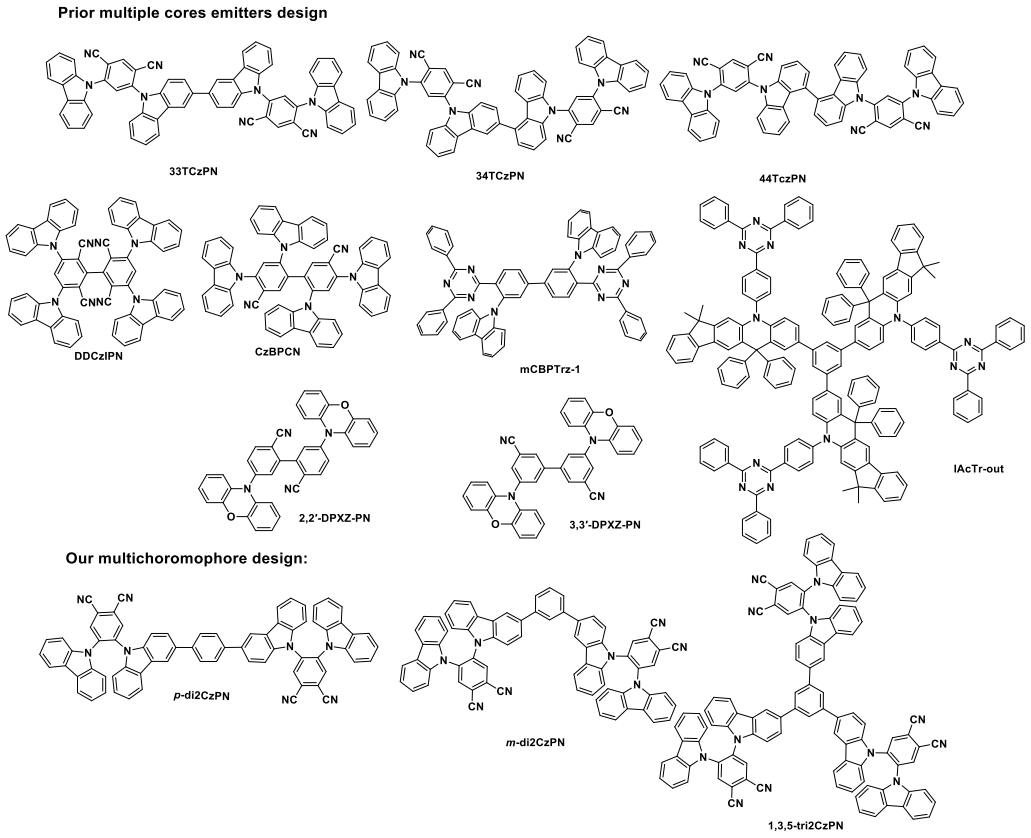

Figure **1.** Multichoromophore molecular structures discussed in this paper.

Results and Discussion

Synthesis

Three multi-donor structures were synthesized first (Scheme **1**). Carbazole was regioselectively brominated using NBS in acetonitrile (MeCN),[37] and then the carbazole was protected as its *N*-tri*iso*propylsilyl ether.[38] **3-BrTIPSCz** was converted to **3-BpinTIPSCz** under palladium-catalysed Miyaura borylation conditions.[39,40] This intermediate was then reacted with 1,4-dibromobenzene, 1,3-dibromobenzene or 1,3,5-tribromobenzene under Suzuki-Miyaura coupling conditions. The crude products were washed with a tetrabutylammonium fluoride (TBAF) solution to afford, respectively, **para-2Cz**, **meta-2Cz** and **tri-3Cz** in moderate yield (~ 55%).

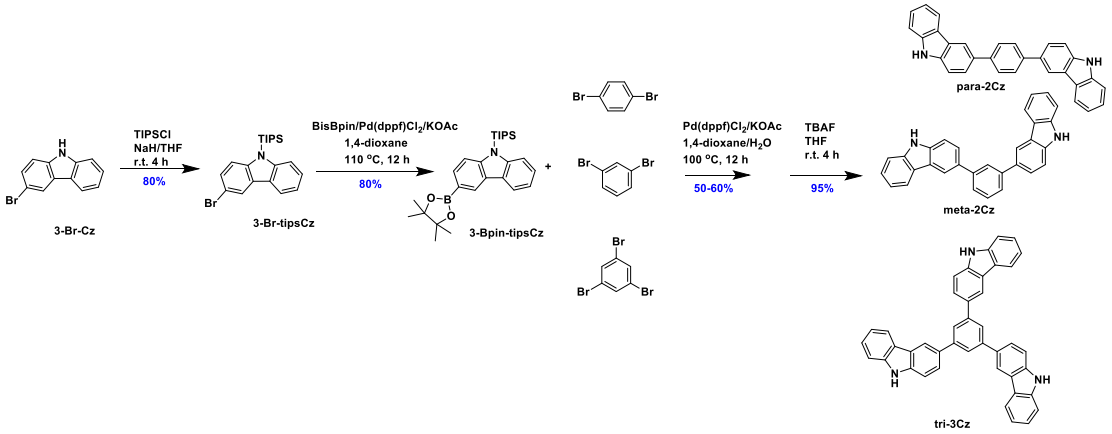

Scheme **1**. Synthesis of multi-carbazole donor intermediates.

CzFPN was synthesized by an S_NAr reaction between carbazole and 4,5-difluorophthalonitrile in good yield (80%). The three multichromophore emitters ***p*-di2CzPN, *m*-di2CzPN** and **1,3,5-tri2CzPN** were obtained in good yield (~55%) from the S_NAr reaction of **CzFPN** with **para-2Cz, meta-2Cz** or **tri-3Cz**. The identity and purity of the three emitters were verified by a combination of melting point, determination ^{1}H NMR, ^{13}C NMR, HRMS, elemental analysis and HPLC analysis.

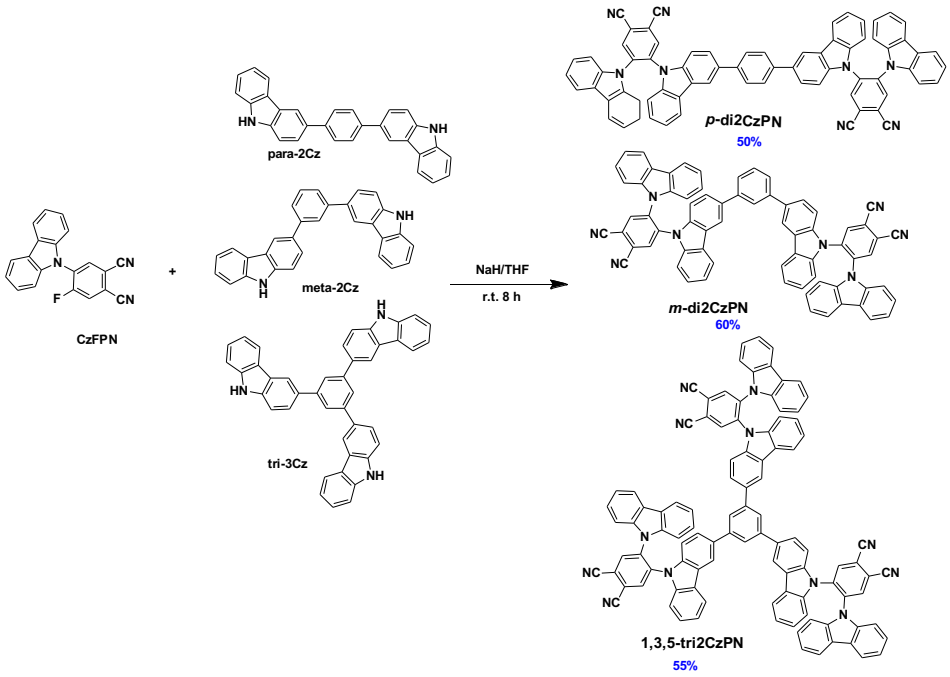

Scheme **2**. Synthesis of multichromophore emitters.

Theoretical calculations

To gain insight into their optoelectronic properties, we performed density functional theoretical (DFT) calculations and time-dependent DFT calculations using the Tamm-Dancoff approximation (TDA-DFT) calculations on ***p*-di2CzPN, *m*-di2CzPN, 1,3,5-tri2CzPN** and the reference compound, **2CzPN**.[41] The ground state, singlet and triplet excited state geometries were calculated in the gas phase using PBE0/6-31g(d, p).[42,43] As shown in Figure **2**, the HOMO of **2CzPN** is localized on the two carbazoles and the central benzene while the LUMO is localized on the phthalonitrile moiety. For the multichoromophore emitters, due to the extended conjugation, the HOMOs are delocalized across the carbazole-phenyl-carbazole motif and the LUMOs are located on the phthalonitrile moieties. The small overlap between HOMO and LUMO ensures that the three emitters possess small ΔE_{ST} values. Due to the extended conjugation of the linked carbazole moieties, the HOMOs of ***p*-di2CzPN, *m*-di2CzPN,** and **1,3,5-tri2CzPN** are destabilized by 0.24, 0.07, and 0.02 eV, respectively, compared to **2CzPN**, and the LUMOs are stabilized by 0.09 , 0.14, and 0.21, respectively, compared to **2CzPN**. As a result, the HOMO-LUMO gap (ΔE_g) of ***p*-di2CzPN, *m*-di2CzPN,** and **1,3,5-tri2CzPN** are reduced to 3.38, 3.50, and 3.49 eV, respectively, compared to 3.71 eV of **2CzPN**. TDA-DFT calculations indicate that the energies of the S_1 state of the three emitters are stabilized by 0.18, 0.15, and 0.10 eV compared to **2CzPN** while there is only a modest change in the energies of the T_1 state, thereby leading to smaller ΔE_{ST} values. The natural transition orbital (NTO) analysis of the three multichoromophore (Figure **S38–40**), show that the transitions to T_1 is

localized to one emitting core and is similar to the T_1 transition of **2CzPN**; the highest occupied NTO (HONTO) is distributed on whole molecule while the lowest unoccupied NTO (LUNTO) is located on the phthalonitrile moiety. The transition to S_1 for the three multichoromophores also only involve one emitting core, where the HONTOs are located on the two carbazoles moieties and the central phenyl ring, and the LUNTOs are localized on the phthalonitrile moiety. The magnitude of the stabilization of the S_1 state is proportional to the degree of conjugation present about the central benzene scaffold as shown in Figure **2**. The ΔE_{ST} values for three emitters are 0.22 eV (***p*-di2CzPN**), 0.25 eV (***m*-di2CzPN**), and 0.28 eV (**1,3,5-tri2CzPN**), compare to 0.34 eV of **2CzPN**. According to the TDA-DFT calculations, the multichoromophore structures possess manifold intermediate triplets between S_1 and T_1 due in part to the slightly differing CT states in each of the cores. Take **1,3,5-tri2CzPN** for example (Figure **S40**), TDA-DFT calculations predict five intermediate triplet states below S_1, while for **2CzPN** (Figure **S37**) only one intermediate triplet state below S_1 exists. The smaller ΔE_{ST} values and the greater density of intermediate triplet states for the three multichoromophore emitters can lead to multiple RISC transition channels via intermediate triplets to S_1, leading to a more efficient RISC process than is present in the reference emitter **2CzPN**. Importantly, TDA-DFT calculation also showed that the transitions involved in the S_1 state of the three multichoromophore emitters have much stronger *f*, compared to **2CzPN** (Table **S1**), which is predictive of a higher radiative rate constant that would be evidenced by a higher Φ_{PL}.

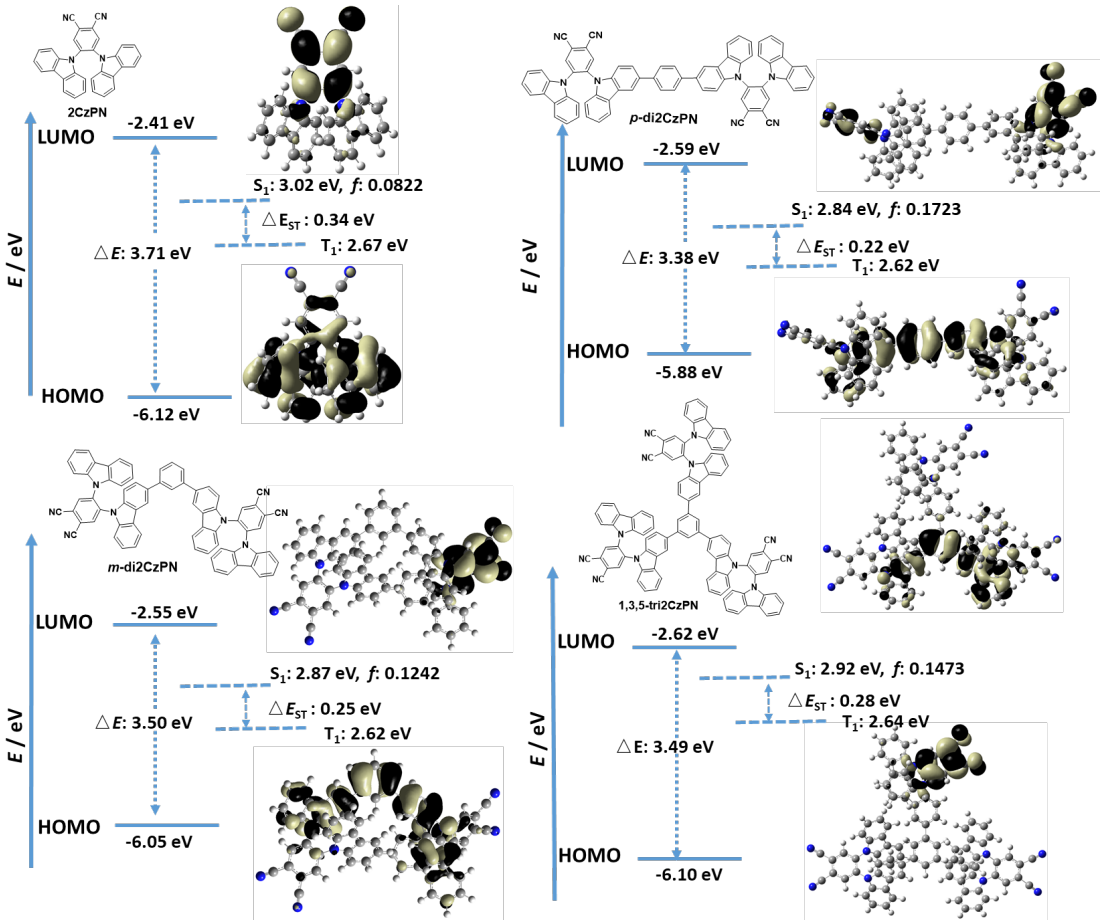

Figure **2**. Theoretical modelling of the energies of the HOMO/LUMO and the S_1 and T_1 states of ***p*-di2CzPN**, ***m*-di2CzPN**, **1,3,5-tri2CzPN**, and reference compound **2CzPN** in the gas phase and the electron density distribution of the frontier molecular orbitals (isovalue = 0.02).

Electrochemistry

Cyclic voltammetry (CV) and differential pulse voltammetry (DPV) were measured in MeCN with *n*-Bu_4NPF_6 as the supporting electrolyte in order to experimentally ascertain HOMO and LUMO energy levels, of the three emitters and **2CzPN** (Figure **3**). The three emitters and **2CzPN** exhibited pseudo-reversible reduction waves and broad, irreversible oxidation waves. The DPV results indicated the three emitters have single electron reduction processes and no further reduction waves were observed scanning from −2 V, which are ascribed to reduction of

one of the phthalonitriles while there are a series of closely related carbazole-based oxidation waves. The first oxidation peaks from DPVs for **2CzPN**, ***p*-di2CzPN**, ***m*-di2CzPN**, and **1,3,5-tri2CzPN** are 1.22, 1.23, 1.38, and 1.40 V vs SCE, while the reduction peaks are −1.71, −1.42, −1.39, and −1.44 V vs SCE, respectively. The HOMO and LUMO values were inferred from the peaks of the oxidation and reduction waves in the DPVs, respectively. The HOMO energies for **2CzPN**, ***p*-di2CzPN**, ***m*-di2CzPN**, and **1,3,5-tri2CzPN** were determined to be −5.64, −5.65, −5.80, and −5.82 eV, respectively. The HOMO energies of the emitters are slightly stabilized (~ 0.2 eV) than those predicted by the DFT calculations yet reproduce the trends observed, while the HOMO energy of **2CzPN** is much more stabilized (0.48 eV) than DFT-predicted calculation. The LUMO energies for **2CzPN**, ***p*-di2CzPN**, ***m*-di2CzPN**, and **1,3,5-tri2CzPN** were determined to be −2.71, −3.00, −3.03, and −2.98 eV, respectively, which are moderately stabilized (~ 0.4 eV) than those predicted by the DFT calculations. The more stabilized LUMOs of the three multichoromophores than **2CzPN** matched the trend predicted by the DFT calculation.

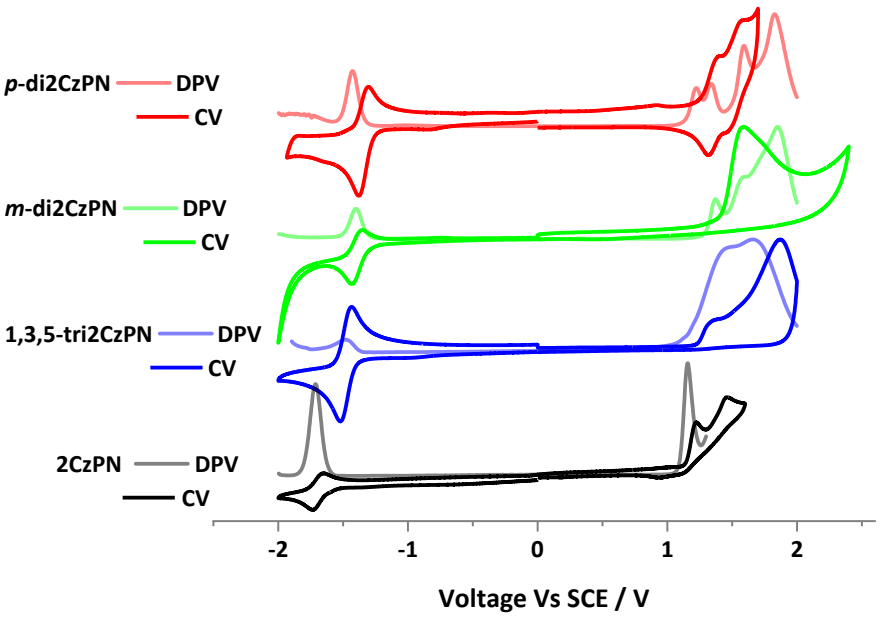

Figure **3.** CV and DPV curves of **2CzPN**, ***p*-di2CzPN**, ***m*-di2CzPN**, and **1,3,5-tri2CzPN** in MeCN with 0.1 M *n*-Bu_4NPF_6 as the supporting electrolyte. Measured condition: scan rate 0.1 V/s, calibrated against a Fc/Fc^+ redox couple and referenced versus SCE.[44]

Photophysical Properties

The photophysical properties of ***p*-di2CzPN**, ***m*-di2CzPN**, and **1,3,5-tri2CzPN** were next investigated both in solution and in thin films. The photophysical properties of the three emitters are summarized in Table **1**. Room-temperature ultraviolet-visible (UV-vis) absorption and PL spectra of ***p*-di2CzPN**, ***m*-di2CzPN**, and **1,3,5-tri2CzPN** and the reference compound **2CzPN** in dilute toluene solution are shown in Figure **4**. According to the TDA-DFT calculations (Table **S2**–**S4**), all four compounds exhibited high intensity locally excited transitions between 280 to 340 nm and intramolecular charge-transfer (ICT) transition absorption bands in the range from 360 to 440 nm. The ICT absorption bands of ***p*-di2CzPN**, ***m*-di2CzPN**, and **1,3,5-tri2CzPN** are much stronger compared to that of **2CzPN**. The molar absorptivity coefficient (ε) for the ICT band of **2CzPN** at 380 nm is 1.2×10^4 M^{-1} cm^{-1} while for ***p*-di2CzPN**, ***m*-di2CzPN**, and **1,3,5-tri2CzPN**, ε increases to 2.5×10^4, 2.5×10^4, and 3.82×10^4 M^{-1} cm^{-1}, respectively, which is proportial to the number of emitter units. The optical bandgaps (E_{opt}), determined from the intersection point of the normalized absorption and emission spectra, of **2CzPN**, ***p*-di2CzPN**, ***m*-di2CzPN**, and **1,3,5-tri2CzPN** are 2.99, 2.85, 2.89, and 2.92 eV, respectively (Figure **S42d**). The λ_{PL}s for **2CzPN**, ***p*-di2CzPN**, ***m*-di2CzPN**, and **1,3,5-tri2CzPN** are 475, 494, 485, and 484 nm in toluene. The nearly identical emission profiles for ***m*-di2CzPN**, and **1,3,5-tri2CzPN** match our NTO analysis where the transitions to the S_1 states are mainly located on one of the

2CzPN moieties in addition to a small contribution from the central benzene ring for both emitters (Figure **S39** and **S40**). For ***p*-di2CzPN**, the electron density distribution is located not only on one of the **2CzPN** moieties but the carbazole at the *para* position is also involved in the transition to S_1 state (Figure **S38**), contributes to the stabilization of the S_1 state and causes the red-shifted emission of ***p*-di2CzPN**. To corroborate the ICT nature of the emission, we measured the PL spectra in solvents of varying polarity. In each case, as the polarity of the solvent increased the PL spectrum red-shifted and broadened, thereby showing a strong positive solvatochromism (Figure **S42**).

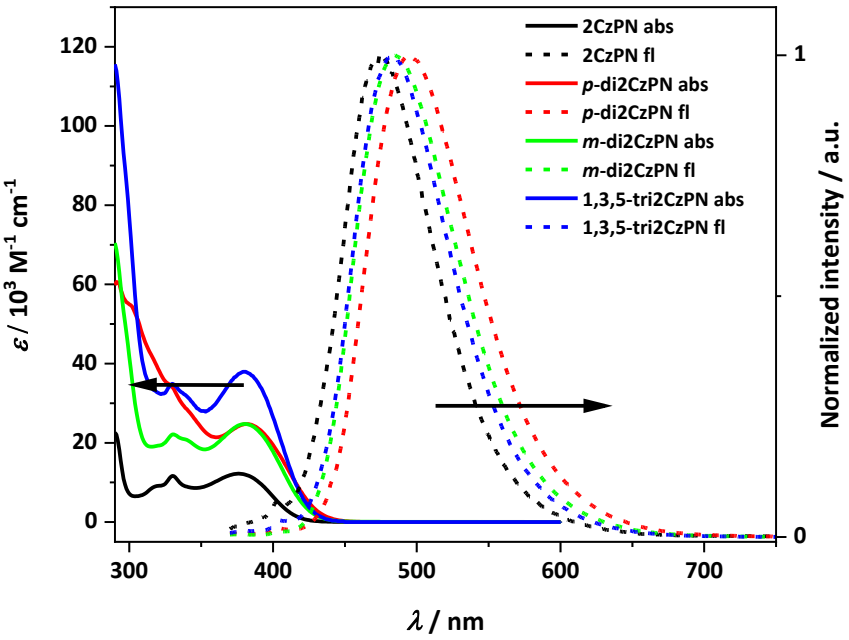

Figure **4**. Absorption and normalized emission spectra of **2CzPN**, ***p*-di2CzPN**, ***m*-di2CzPN**, and **1,3,5-tri2CzPN** in toluene solution (10^{-5} M). λ_{exc} = 355 nm.

The three emitters exhibited near quantitative Φ_{PL} in toluene, values that were strongly quenched under aerated conditions. For ***p*-di2CzPN**, ***m*-di2CzPN**, and **1,3,5-tri2CzPN** in

aerated toluene, the Φ_{PL} values were 39%, 27% and 34%, respectively, while under oxygen-free conditions the Φ_{PL} values reached, respectively, 98%, 96% and 99%. These compounds are thus significantly more emissive than **2CzPN,** with Φ_{PL} of 26% in aerated and 28% in oxygen-free toluene.[45] The oxygen sensitivity is an indication of accessible triplet excited states, and is a frequent characteristic of TADF emitters. We next measured the time-resolved emission decays in toluene. Each of the three emitters exhibit a prompt decay component with the lifetime in the nanosecond region and bi-exponential delayed decay kinetics with the lifetimes in the microsecond region (Figure **S43**). The prompt decay lifetimes (τ_p) for ***p*-di2CzPN**, ***m*-di2CzPN**, and **1,3,5-tri2CzPN** are 13.4, 15.0, and 14.9 ns, respectively, while the average delayed decay lifetimes ($\tau_{d,avg}$) are 2.4 μs for ***p*-di2CzPN**, 22.2 μs for ***m*-di2CzPN**, and 58.2 μs for **1,3,5-tri2CzPN**. Compared to the emission decay of **2CzPN** (24.4 ns (99.5%) and 1.1 μs (0.5%)),[45] the three multichoromophore emitters exhibited longer delayed lifetime and a significantly increased delayed component in toluene.

We next investigated the photophysical properties of the three emitters in 10 wt% doped PMMA films as the polarity of PMMA closely mimics that of toluene.[46] The ***m*-di2CzPN** and **1,3,5-tri2CzPN** compounds showed slightly red-shifted emission maxima compared to those in toluene at 498 and 494 nm, respectively while the peak for ***p*-di2CzPN** was red-shifted to 516 nm (Figure **5**). The Φ_{PL} values under N_2 for **2CzPN**, ***p*-di2CzPN**, ***m*-di2CzPN** and **1,3,5-tri2CzPN** are 76%,[45] 64%, 77% and 78%, respectively. The time-resolved emission decays were obtained under oxygen-free conditions (Figure **S44**). Similar to the profiles in toluene, the τ_p values for ***p*-di2CzPN**, ***m*-di2CzPN**, **and 1,3,5-tri2CzPN** are 29, 38, and 26 ns, respectively,

which are slightly longer than that of **2CzPN** (18 ns). The $\tau_{d,avg}$ values are 286.3 μs for ***p*-di2CzPN**, 311.0 μs for ***m*-di2CzPN**, 262.4 μs for **1,3,5-tri2CzPN**, respectively, which are much shorter than the $\tau_{d,avg}$ of **2CzPN** in PMMA film (1.5 ms).[45]

Prompt fluorescence and phosphorescence spectra were obtained by time-resolved emission spectroscopy (TRES) measurement in 10 wt% doped PMMA at 77 K. The prompt emission spectrum of each emitter exhibited continuous red-shifting from 1 ns to 100 ns, which could be ascribed to the energetic relaxation of molecular vibration and rotation (Figure **S45**).[47] The phosphorescence spectra were obtained from integration of the TRES spectrum from 2 ms to 9 ms (Figure **S45**). The room temperature emission spectra of ***p*-di2CzPN**, ***m*-di2CzPN**, and **1,3,5-tri2CzPN** are ca. 20 nm red-shifted and are slightly broader compared to their corresponding prompt fluorescence spectra measured at 77 K. We calculated the energy of the singlet state from the onset of the fluorescence spectra from 1 ns and the energy of the triplet state from the onset of the phosphorescence spectra from 2 ms (Figure **5**). The S_1 energies for ***p*-di2CzPN**, ***m*-di2CzPN**, and **1,3,5-tri2CzPN** were calculated to be 2.96, 3.01, and 3.00 eV, respectively, which closely match those of the TDA-DFT calculation, while the T_1 state was found at 2.80, 2.90, and 2.91 eV, respectively, which are slightly destabilized compared to those calculated by TDA-DFT. The ΔE_{ST} values for ***p*-di2CzPN**, ***m*-di2CzPN**, and **1,3,5-tri2CzPN** are 0.16, 0.11, and 0.09 eV, which are reduced compared to 0.21 eV for **2CzPN** in PMMA film.[45] These small ΔE_{ST} values are consistent with an efficient TADF process, which are consistent with the shorter delayed lifetimes of the three multichoromophore emitters in the doped PMMA films.

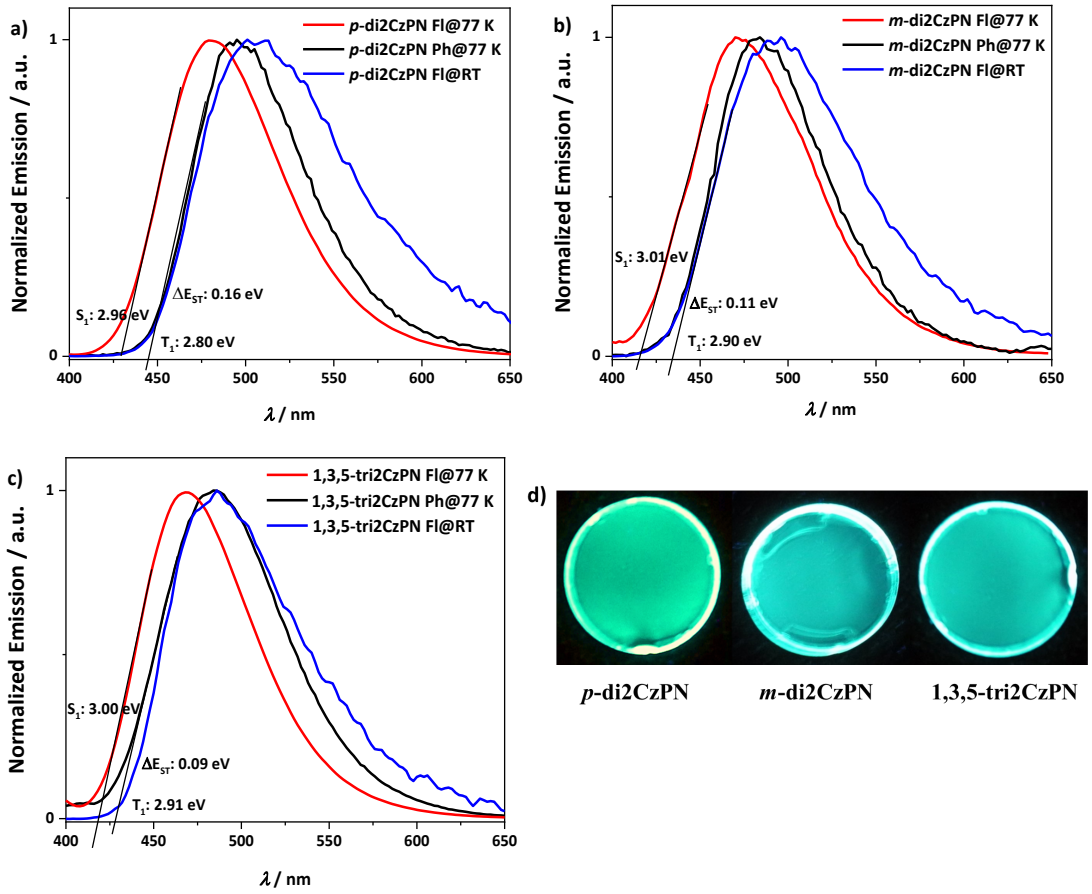

Figure **5.** Fluorescence (Fl) and phosphorescence (Ph) spectra of 10 wt% PMMA films of (a) ***p*-di2CzPN**, (b) ***m*-di2CzPN**, and (c) **1,3,5-tri2CzPN** at 77 K. (d) Photos of 10 wt% PMMA films of ***p*-di2CzPN**, ***m*-di2CzPN**, and **1,3,5-tri2CzPN**. The fluorescence spectra were sliced from 1 ns to 100 ns while the phosphorescence spectra were sliced from 2 ms to 10 ms (λ_{exc} = 378 nm).

Table **1.** Key Photophysical data of ***p*-di2CzPN**, ***m*-di2CzPN**, **1,3,5-tri2CzPN** and **2CzPN**.

Compound	λ_{abs} **(ε)[a] / nm (/ 10^3 m^{-1} cm^{-1})**	λ_{PL} **/ nm**	Φ_{PL} **/ %**	$S_1/T_1/\Delta E_{ST}$[d] **/ eV**	τ_p **/ ns**	$\tau_{d,avg}$ **/ µs**	**HOMO/LUMO/** ΔE_g[f] **/ eV**
***p*-di2CzPN**	326 (35),	494[a]/	39/98[a]	2.96/2.80	13[a]	2.4[a]	−5.65/−3.00/
	382 (25)	516[b]	52/64[c]	/0.16	29[e]	286.3[e]	2.65
***m*-di2CzPN**	332 (22),	485[a]/	27/96[a]	3.01/2.90	15[a]	22.2[a]	−5.80/−3.03/
	381 (25)	498[b]	59/77[c]	/0.11	38[e]	311.0[e]	2.77
1,3,5-	330 (35),	483[a]/	34/99[a]	3.00/2.91	15[a]	58.2[a]	−5.82/−2.98/
tri2CzPN	381 (38)	494[b]	58/78[c]	/0.09	26[e]	262.4[e]	2.84
2CzPN[45]	329 (12),	475[a]	26/28	2.88/2.67	22[a]	1.1[a]	−5.64/−2.71/
	364 (11)	492[b]	63/76	/0.21	18[e]	1500[e]	2.93

[a] Measured in toluene solution (λ_{exc} = 378 nm), [b] Measured in 10 wt% doped PMMA films (λ_{exc} = 378 nm), [c] Measured using an integrating sphere of 10 wt% doped PMMA films under air/N_2 (λ_{exc} = 360 nm), [d] S_1 is obtained from the onset of the prompt emission measured at 77 K, T_1 is obtained from the onset of the phosphorescence spectrum measured at 77 K, $\Delta E_{ST} = S_1 - T_1$, [e] τ_p (prompt lifetime) and $\tau_{d,avg}$ (average delayed lifetime) were obtained from the transient PL decay of doped film under vacuum, λ_{exc} = 378 nm, measure region: 50 µs and 4 ms, [f] HOMO and LUMO values were obtained from the redox potentials from the DPV, $E_{HOMO/LUMO} = -(E_{ox/red} + 4.8)$ where $E_{ox/red}$ are from DPV scan corrected vs Fc/Fc^+, $\Delta E_g = E_{LUMO} - E_{HOMO}$.[44]

To corroborate the TADF character of the three emitters in doped PMMA films, we measured the temperature-dependent time-resolved decay spectra (Figure **6**). In each case, the delayed fluorescence increased with increasing temperature, which is a hallmark of TADF as the RISC process becomes suppressed at low temperatures.

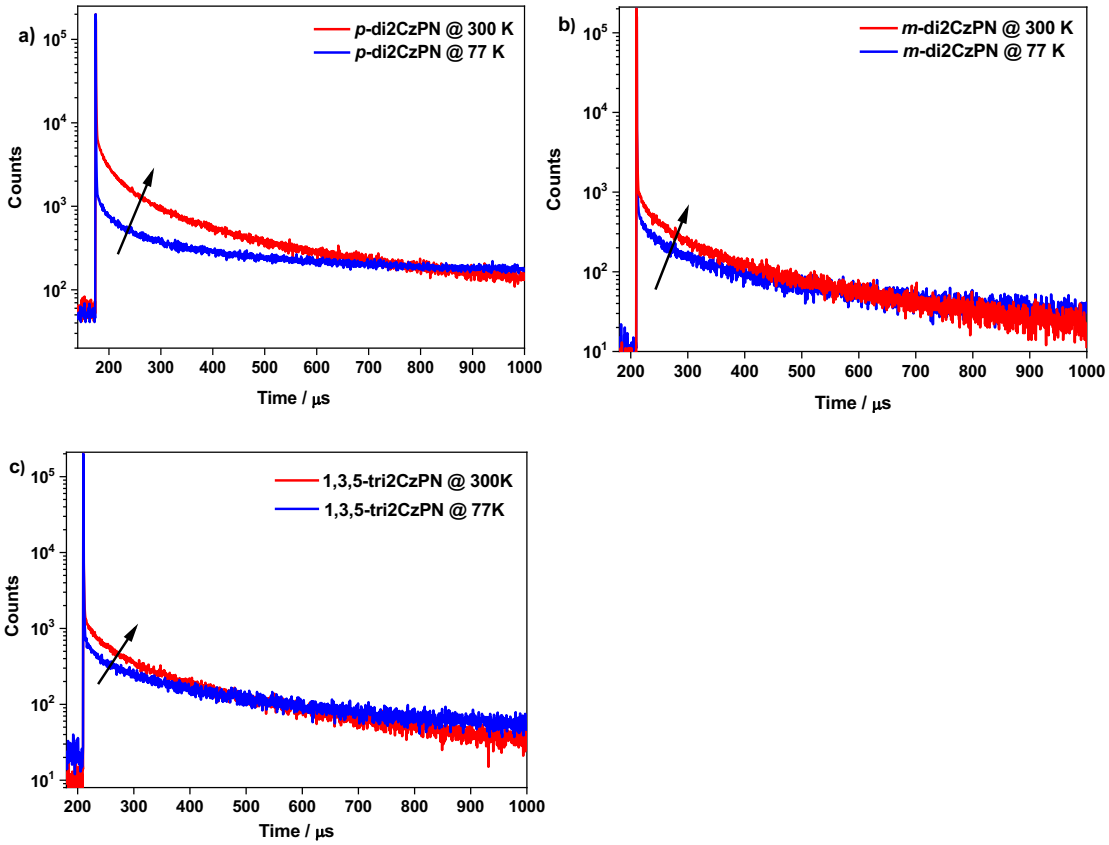

Figure **6.** Temperature-dependent time-resolved PL decay spectra of 10 wt% doped PMMA films of (a) ***p*-di2CzPN**, (b) ***m*-di2CzPN**, and (c) **1,3,5-tri2CzPN**. (λ_{exc} = 378 nm, time region: 1 ms)

The kinetics of the three multichoromophore emitters and the reference emitter **2CzPN** were investigated in 10 wt% doped bis[2-(diphenylphosphino)phenyl] ether oxide (DPEPO) films for ***p*-di2CzPN**, ***m*-di2CzPN**, and **2CzPN**, and a 20 wt% doped CBP film for **1,3,5-tri2CzPN** (Figure **7**, Table **2**). The three emitters all exhibit high Φ_{PL} values in host matrices suitable for OLEDs. The prompt lifetimes for ***p*-di2CzPN**, ***m*-di2CzPN**, and **1,3,5-tri2CzPN** are comparable to the 20 ns of **2CzPN**, and τ_d values are much shorter than the 137 μs of **2CzPN**. (Table **2**) The k_{RISC} values for ***p*-di2CzPN**, ***m*-di2CzPN**, and **1,3,5-tri2CzPN** are calculated to be 1.1 × 10^5, 0.7 × 10^5, and 1.7 × 10^5 s^{-1}, respectively, which are faster than **2CzPN** (0.3 × 10^5

s^{-1}). **1,3,5-tri2CzPN** exhibits the fastest k_{RISC} value, which is ascribed to the small ΔE_{ST} and the greater density of intermediate triplet states predicted by TDA-DFT calculation.

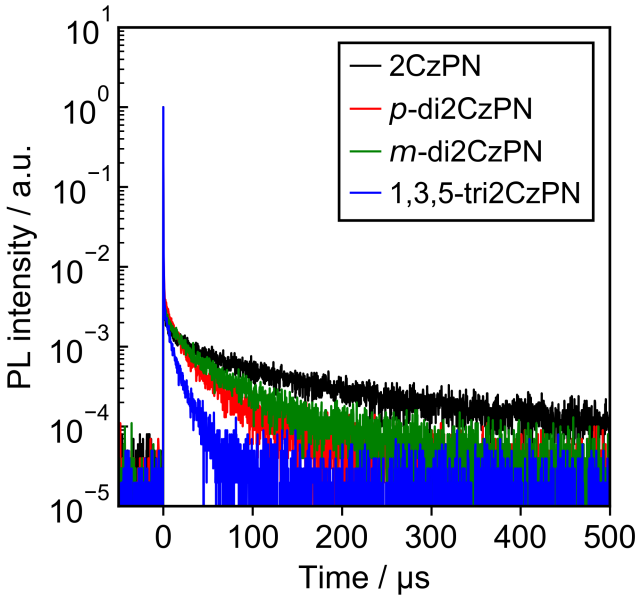

Figure **7**. PL decay spectra of 10 wt% doped DPEPO films of **2CzPN**, ***p*-di2CzPN**, ***m*-di2CzPN**, and a 20 wt% doped CBP film of **1,3,5-tri2CzPN** (λ_{exc} = 280 nm).

Table **2**: Exciton lifetime and the kinetic constants of ***p*-di2CzPN**, ***m*-di2CzPN** and **1,3,5-tri2CzPN** in host materials. Φ_{PL}, τ_p, and τ_d are measured under inert atmosphere.

compound	matrix	λ_{PL} / nm	Φ_{PL} / %	Φ_p / %	Φ_d / %	τ_p / ns	τ_d / µs	k_r^s /10^7 s^{-1}	k_{ISC} / 10^7 s^{-1}	k_{RISC} / 10^5 s^{-1}
***p*-di2CzPN**	10 wt% in DPEPO	531	59	21	39	18	25.7	1.2	3.7	1.1
***m*-di2CzPN**	10 wt% in DPEPO	510	70	22	48	17	44.2	1.3	4.0	0.7
1,3,5-tri2CzPN	20 wt% in CBP	505	54	32	22	21	9.8	1.5	2.0	1.7
2CzPN	10 wt% in DPEPO	496	98	21	77	20	137	1.1	4.0	0.3

Electroluminescence Properties

A solution-processed OLED based on **1,3,5-tri2CzPN** was fabricated using the architecture: Indium tin oxide (ITO) (50 nm)/poly(3,4-ethylenedioxythiophene) polystyrene sulfonate (PEDOT:PSS) (35 nm)/20 wt% **1,3,5-tri2CzPN**:CBP/1,3-bis[3,5-di(pyridin-3-yl)phenyl] benzene (BmPyPhB) (30 nm)/lithium quinolin-8-olate (Liq) (1 nm)/Al (80 nm). PEDOT:PSS layer and the emitting layer were deposited by spin-coating process and the other layers were thermally vacuum-deposited. The performance of the device is summarized in Figure **8**. The turn-on voltage for the device is 5.6 V and the device exhibits sky-blue emission with the peak maximum wavelength at 500 nm with CIE of (0.22, 0.44) and EQE_{max} of 7.1 % at 0.1 mA cm^{-2}, while the maximum luminance reaches 1,000 cd m^{-2}. Compared with the PL spectrum of a 20 wt% **1,3,5-tri2CzPN**:CBP film, the EL spectrum narrowed as shown in Figure **S46**. This narrowing of the EL spectrum might be attributed to the so-called micro-cavity effect resulting from the optical interference of emitted irradiance in the OLED. Considering the Φ_{PL} of **1,3,5-tri2CzPN** in CBP (54%), the EQE_{max} of 7.1% from device is close to the theoretical EQE_{max} of

10.8% under the assumption that (1) the charge balance is unity; (2) the efficiency of radiative exciton production is unity, and (3) the light out-coupling efficiency is 0.2. The device suffers severe efficiency roll-off as the EQE decreases to 1% at 10 mA cm^{-2}.

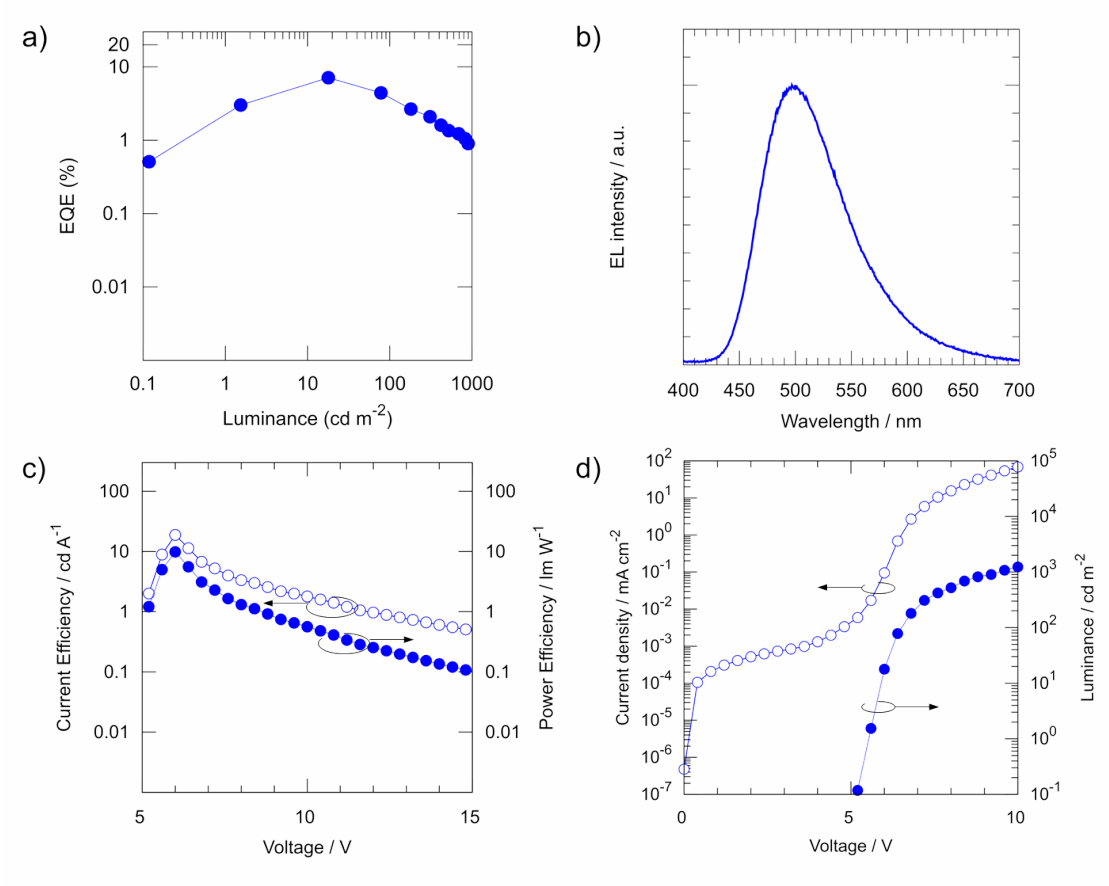

Figure **8**. (a) EQE-luminance characteristics, (b) EL spectrum, (c) current efficiency-voltage-power efficiency properties and (d) current density-voltage-luminance properties of the 1,3,5-tri2CzPN based OLED.

Conclusions

By connecting TADF emitting core **2CzPN** to a central benzene ring, three multichromophore emitters, ***p*-di2CzPN**, ***m*-di2CzPN** and **1,3,5-tri2CzPN**, were synthesized and characterized. The multichromophore molecular structure results in an improved molar

extinction coefficient for the low-energy charge transfer states and near unity photoluminescence quantum yield values in solution. TDA-DFT calculations showed that density intermediate triplet states between S_1 and T_1 could contribute to an improved TADF efficiency. The three emitters exhibit smaller ΔE_{ST} values leading to fast delayed lifetimes in doped films. The k_{RISC} for **1,3,5-tri2CzPN** reaches 1.7×10^5 s^{-1}, which is more than five times faster than **2CzPN** (0.3×10^5 s^{-1}), while the k_{RISC} for ***p*-di2CzPN** and ***m*-di2CzPN** are more than three and two times faster than **2CzPN**, respectively. A solution-processed OLED based on **1,3,5-tri2CzPN** shows a sky-blue emission with CIE coordinates of (0.22, 0.44) and achieves an EQE_{max} of 7.1%. This work demonstrates that the multichromophore molecular design is a practical route to improve simultaneously the Φ_{PL} and RISC efficiency.

Experimental section

General consideration

All experiments were carried out with commercial solvents from Fisher Scientific Ltd, except where specifically mentioned. Commercially obtained chemicals were used as received. All manipulations were carried out under an inert atmosphere using standard Schlenk line techniques.

^{1}H NMR, and ^{13}C NMR were recorded at room temperature on a Bruker Avance spectrometer at 400 MHz and 101 MHz or 500 MHz and 126 MHz, respectively. ^{1}H NMR and ^{13}C NMR spectra were referenced to the residual solvent peaks ($CDCl_3$ = 7.26 ppm for ^{1}H NMR and 77.16 ppm for ^{13}C NMR, d_6-DMSO = 2.50 ppm for ^{1}H NMR and 29.84 ppm for ^{13}C NMR, respectively). The following abbreviations have been used for multiplicity assignments: “s” for

singlet, “d” for doublet, “t” for triplet, “m” for multiplet and “br” for broad. Elemental analysis was measured by London Metropolitan University. Samples for high resolution mass spectrum (HRMS) were sent to the National Mass Spectrometry Facility in Swansea (EPSRC) for analysis by nano-electrospray on an Orbitrap instrument.

Materials and synthesis

Synthesis of 3-bromide-Carbazole (3-BrCz)

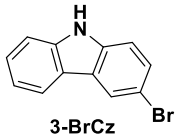

3-BrCz

3-BrCz was synthesized according to the literature.[38] To a 250 mL flask, carbazole (1.7 g, 10 mmol, 1 equiv.) was dissolved in 10 mL of acetonitrile and cooled down in ice-water bath. The acetonitrile solution of *N*-bromosuccinimide (1.7 g, 11 mmol, 1.1 equiv.) was added into the carbazole solution dropwise. The mixture was stirred for 4 h at room temperature and washed with water and extracted with dichloromethane (DCM) three times (30 mL×3). The organic solvent was removed under reduced pressure. The crude product was recrystallized in DCM and hexane (1/20) to obtain **3-BrCz** as white solid powder.

Yield: 90%. $\mathbf{R_f}$ = 0.46 (20% DCM/Hexane). **Mp**: 195-197 ºC (Lit. Mp.[38] 197-198 ºC). **^{1}H NMR (400 MHz, d_6-DMSO) δ (ppm):** 11.44 (s, 1H), 8.36 (d, *J*=1.9 Hz, 1H), 8.16 (d, *J*=7.8 Hz, 1H), 7.56-7.37 (m, 4H), 7.24-7.09 (m, 1H). **^{13}C{^{1}H} NMR (101 MHz, d_6-DMSO) δ (ppm):** 140.5, 138.7, 128.2, 126.7, 124.7, 123.1, 121.8, 121.0, 119.3, 113.2, 111.5, 110.9. **LRMS** (ESI) m/z: **[M-H]$^-$ Calcd for $C_{12}H_7BrN$** 245.98; **Found** 246.08. The characterization matches that previously reported.[38]

Synthesis of 3-bromo-9-(triisopropylsilyl)-9*H*-carbazole (3-Br-tipsCz)

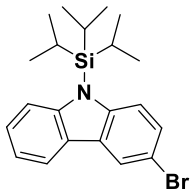

3-Br-tipsCz

To a 250 mL flask, sodium hydride (500 mg, 12 mmol, 1.2 equiv.) was added and the flask was degassed by three cycles of vacuum-nitrogen purging. Then **3-BrCz** (2.5 g, 10 mmol, 1 equiv.) was dissolved in 20 mL of THF and added into the flask dropwise. After the mixture was stirred for 30 min in ice-water bath, chlorotriisopropylsilane (TIPSCl) (2.9 g, 15 mmol, 1.5 equiv.) dissolved in 20 mL of THF was added dropwise into the solution. The mixture was warmed up to room temperature and stirred for 8 h. A trace of water was injected to the mixture to quench the reaction. The mixture was washed with water and extracted with DCM three times (50 mL ×3). The organic solvent was removed under reduced pressure and the crude product was purified by column chromatography. DCM/Hexane=1/10 was used as eluent to obtain **3-Br-tipsCz** as a white wax solid.

Yield: 80%. $\mathbf{R_f}$: 0.66 (10% DCM/Hexane) **Mp:** 37-40 ºC. **^{1}H NMR (400 MHz, $CDCl_3$) δ (ppm):** 8.19 (d, *J* = 2.2 Hz, 1H), 8.04 (d, *J* = 7.7 Hz, 1H), 7.71 (d, *J* = 8.5 Hz, 1H), 7.58 (dd, *J* = 9.0 Hz, 2.4Hz, 1H), 7.49 -7.40 (m, 2H), 7.28 -7.22 (m, 1H), 2.25 - 1.77 (m, 3H), 1.21 (d, *J* = 7.5 Hz, 18H). **^{13}C{^{1}H} NMR (101 MHz, $CDCl_3$) δ (ppm):** 145.4, 143.7, 128.5, 127.8, 126.0, 125.4, 122.4, 119.9, 115.5, 114.2, 112.4, 18.6, 13.8. **HRMS** (ESI) m/z: **$[M+H]^+$ Calcd for $C_{21}H_{28}BrNSi$** 402.1249; **Found**: 402.1247.

Synthesis of 3-(4,4,5,5-tetramethyl-1,3,2-dioxaborolan-2-yl)-9-(triisopropylsilyl)-9H-carbazole (3-Bpin-tipsCz)

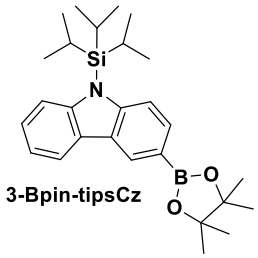

3-Bpin-tipsCz

To a 100 mL flask were added **3-Br-tipsCz** (400 mg, 1 mmol, 1 equiv.), bis(pinacolato)diboron (300 mg, 1.2 mmol, 1.2 equiv.), 1,1′-bis(diphenyl-phosphino)ferrocene]dichloro palladium (II) (100 mg, 0.1 mmol, 0.1 equiv.), potassium acetate (990 mg, 10 mmol, 10 equiv.), and 20 mL of 1,4-dioxane. The mixture was degassed via three times of freeze-pump-thaw cycles and stirred at 110 ºC for 12 h under nitrogen. The mixture was washed with water and extracted with DCM three times (50 mL ×3). The organic solvent was removed under reduced pressure and the crude product was purified by column chromatography. DCM/Hexane=1/3 was used as eluent to obtain **3-Bpin-tipsCz** as a white solid.

Yield: 80%. $\mathbf{R_f}$: 0.44 (25% DCM/Hexane) **Mp:** 51-53 ºC. **^{1}H NMR (400 MHz, $CDCl_3$) δ (ppm):** 8.58 (s, 1H), 8.15 (d, J=2.2 Hz, 1H), 7.85 (dd, *J* = 8.4 Hz, 1.3 Hz, 1H), 7.71 (dd, *J* = 8.5 Hz, 4.1 Hz, 2H), 7.38 (dd, *J* = 8.5 Hz, 7.1 Hz, 1H), 7.28 – 7.23 (m, 1H), 2.02 (m, 3H), 1.21 (d, *J* = 7.5 Hz, 18H). **^{13}C{^{1}H} NMR (101 MHz, $CDCl_3$) δ (ppm):** 147.1, 144.7, 131.9, 131.3, 126.6, 124.8, 120.1, 119.4, 113.6, 110.1, 109.5, 82.9, 24.9, 18.6, 13.8, 12.3. **HRMS** (ESI) m/z: **$[M+H]^+$ Calcd for $C_{27}H_{41}BNO_2Si$** 450.2995; **Found**: 450.2995.

Synthesis of 1,4-bis(9-(triisopropylsilyl)-9*H*-carbazol-3-yl)benzene (para-2tipsCz)

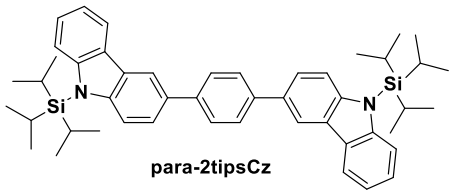

General procedure A

To a 100 mL flask were added **3-Bpin-tipsCz** (1.1 g, 2.5 mmol, 2.5 equiv.), 1,4-dibromonbenzene (235 mg, 1 mmol, 1 equiv.), 1,1′-bis(diphenyl-phosphino)ferrocene]dichloro palladium (II) (100 mg, 0.1 mmol, 0.1 equiv.), potassium carbonate (1.4 g, 10 mmol, 10 equiv.), 20 mL of 1,4-dioxane, and 2 mL of distilled water. The mixture was degassed via three freeze-pump-thaw cycles and stirred at 95 °C for 12 h under nitrogen. The mixture was washed with water and extracted with dichloromethane (DCM) three times (50 mL×3). The organic solvent was removed under reduced pressure and purified by column chromatography. DCM/Hexane=1:5 was used as eluent to obtain **para-2tipsCz** as a white solid.

Yield: 50%. **R_f**: 0.62 (20% DCM/Hexane). **Mp:** 78 °C-81 °C. **^{1}H NMR (500 MHz, $CDCl_3$) δ (ppm):** 8.40 (d, *J* = 2.0 Hz, 2H), 8.19 (dd, *J* = 7.7, 1.4 Hz, 2H), 7.85 – 7.62 (m, 6H), 7.42 (ddd, *J* = 8.5, 7.1, 1.4 Hz, 2H), 7.37 – 7.24 (m, 2H), 2.25 – 1.90 (m, 6H), 1.28 (d, *J* = 7.6 Hz, 36H). **^{13}C{^{1}H} NMR (126 MHz, $CDCl_3$) δ (ppm):** 145.6, 144.2, 133.5, 128.8, 127.4, 127.2, 126.8, 126.2, 125.4, 125.0, 119.9, 119.6, 118.0, 114.3, 18.7, 13.9. **HRMS** (ESI) m/z: **$[M+H]^+$ Calcd for $C_{48}H_{61}N_2Si_2$** 721.4361; **Found**: 721.4368.

Synthesis of 1,3-bis(9-(triisopropylsilyl)-9H-carbazol-3-yl)benzene (meta-2tipsCz)

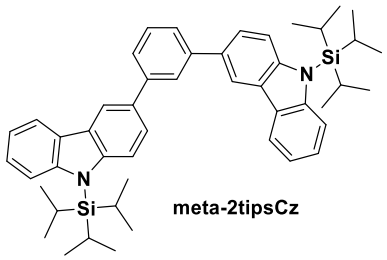

meta-2tipsCz

Synthesized as **General procedure A** to afford **meta-2tipsCz** as a white solid.

Yield: 40%. **R_f**: 0.62 (20% DCM/Hexane). **Mp:** 70 ºC-73 ºC. **^{1}H NMR (500 MHz, $CDCl_3$) δ (ppm):** 8.40 (d, *J* = 2.0 Hz, 2H), 8.17 (dd, *J* = 7.7, 1.4 Hz, 2H), 8.10 (s, 1H), 7.82 (d, *J* = 8.7 Hz, 2H), 7.77 – 7.71 (m, 6H), 7.65 – 7.57 (m, 1H), 7.41 (ddd, *J* = 8.5, 7.0, 1.4 Hz, 2H), 7.29 (d, *J* = 2.4 Hz, 1H), 2.28 – 1.94 (m, 6H), 1.27 (d, *J* = 7.5 Hz, 36H). **^{13}C{^{1}H} NMR (126 MHz, $CDCl_3$) δ (ppm):** 145.6, 144.7, 142.3, 133.0, 129.2, 127.1, 126.6, 126.3, 125.5, 124.9, 119.8, 119.7, 118.2, 114.3, 114.2, 18.7, 13.9. **HRMS** (ESI) m/z: **$[M+H]^+$ Calcd for $C_{48}H_{61}N_2Si_2$** 721.4361; **Found**: 721.4368.

Synthesis of 1,3,5-tris(9-(triisopropylsilyl)-9H-carbazol-3-yl)benzene (tri-3tipsCz)

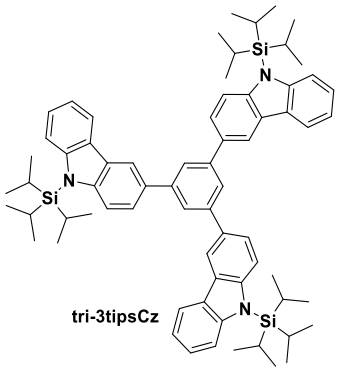

tri-3tipsCz

Synthesized as **General procedure A** to obtain **tri-3tipsCz** as a white solid.

Yield: 45%. **R_f**: 0.60 (15 % DCM/Hexane). **Mp:** 86 ºC-88 ºC. **^{1}H NMR (400 MHz, $CDCl_3$) δ (ppm):** 8.49 (s, 3H), 8.19 (dd, *J* = 7.8, 1.4 Hz, 3H), 8.07 (s, 3H), 7.85 (d, *J* = 1.3 Hz, 6H), 7.76 (d, *J* = 8.5 Hz, 3H), 7.42 (ddd, *J* = 8.5, 7.1, 1.4 Hz, 3H), 7.29 (d, *J* = 7.1 Hz, 3H), 2.48 – 1.84

(m, 9H), 1.28 (d, J = 7.5 Hz, 54H). **$^{13}C\{^{1}H\}$ NMR (101 MHz, $CDCl_3$) δ (ppm):** 145.6, 144.8, 142.8, 133.2, 128.8, 127.2, 126.7, 125.5, 125.0, 124.7, 120.0, 119.7, 118.3, 114.2, 18.7, 13.9. **HRMS** (ESI) m/z: **$[M+H]^+$ Calcd for $C_{69}H_{88}N_3Si_3$** 1042.6288; **Found**: 1042.6281.

Synthesis of 1,4-di(9H-carbazol-3-yl)benzene (para-2Cz)

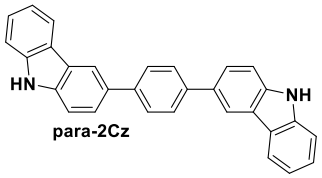

para-2Cz

General procedure B

To a 100 mL flask was added tetrabutylammonium fluoride (TBAF) (600 mg, 2.5 mmol, 2,5 equiv.), and **para-2tipsCz** (720 mg, 1 mmol, 1 equiv.) in 10 mL of THF was slowly added and the mixture stirred at room temperature for 8 h. The reaction mixture was filtered, and the solvent removed under reduced pressure and purified by column chromatography. DCM/Hexane=1/1 was used as eluent to obtained **para-2Cz** as white solid.

Yield: 90%. **R_f**: 0.55 (50% DCM/Hexane) **Mp:** 184 ºC-186 ºC. **^{1}H NMR (400 MHz, d_6-DMSO) δ (ppm):** 11.43 (s, 2H), 8.53 (d, J = 1.8 Hz, 2H), 8.25 (d, J = 7.7 Hz, 2H), 7.90 (s, 4H), 7.79 (dd, J = 8.4, 1.8 Hz, 2H), 7.70 – 7.48 (m, 4H), 7.42 (ddd, J = 8.2, 7.1, 1.2 Hz, 2H), 7.20 (ddd, J = 8.0, 7.1, 1.0 Hz, 2H). **$^{13}C\{^{1}H\}$ NMR (101 MHz, d_6-DMSO) δ (ppm):** 140.7, 139.8, 131.0, 129.3, 127.5, 126.2, 124.9, 123.6, 123.1, 121.0, 119.1, 118.6, 111.8, 111.6. **HRMS** (ESI) m/z: **$[M+H]^+$ Calcd for $C_{30}H_{21}N_2$** 409.1699; **Found**: 409.1700.

Synthesis of 1,3-di(9H-carbazol-3-yl)benzene (meta-2Cz)

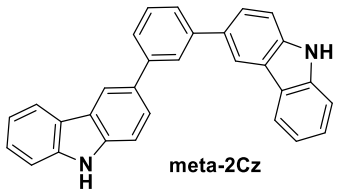

meta-2Cz

Synthesized as **General procedure B**. DCM/Hexane=1/1 was used as eluent to obtained meta-2Cz as white solid.

Yield: 90%. **R_f**: 0.61 (50% DCM/Hexane). **Mp:** 160 ºC-165 ºC. **^{1}H NMR (400 MHz, d_6-DMSO) δ (ppm):** 11.36 (s, 2H), 8.61 (d, *J* = 1.8 Hz, 2H), 8.29 (d, *J* = 7.8 Hz, 2H), 8.15 (s, 1H), 7.86 (dd, *J* = 8.4, 1.8 Hz, 2H), 7.73 (dd, *J* = 7.7, 1.8 Hz, 2H), 7.66 – 7.47 (m, 5H), 7.42 (ddd, *J* = 8.2, 7.0, 1.2 Hz, 2H), 7.20 (ddd, *J* = 8.0, 7.0, 1.0 Hz, 2H). **^{13}C{^{1}H} NMR (101 MHz, d_6-DMSO) δ (ppm):** 142.4, 140.7, 139.8, 132.8, 131.6, 129.9, 126.2, 125.6, 125.4, 123.6, 123.1, 121.1, 119.1, 111.8, 111.6. **HRMS** (ESI) m/z: **$[M+H]^+$ Calcd for $C_{30}H_{21}N_2$** 409.1699; **Found**: 409.1700.

Synthesis of 1,3,5-tri(9*H*-carbazol-3-yl)benzene (tri-3Cz)

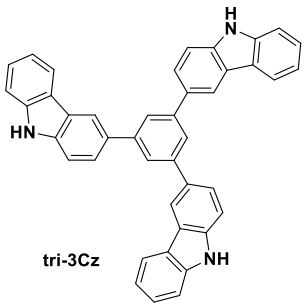

tri-3Cz

Synthesized as **General procedure B**. DCM/Hexane=1/1 was used as eluent to obtained **tri-3Cz** as white solid.

Yield: 90%. **R_f**: 0.46 (50% DCM/Hexane). **Mp:** 173 ºC-176 ºC. **^{1}H NMR (400 MHz, d_6-DMSO) δ (ppm):** 11.41 (s, 3H), 8.74 (s, 3H), 8.33 (d, *J* = 7.8 Hz, 3H), 8.09 (s, 3H), 8.05 – 7.86 (m, 3H), 7.65 (d, *J* = 8.4 Hz, 3H), 7.54 (d, *J* = 8.1 Hz, 3H), 7.42 (t, *J* = 7.7 Hz, 3H), 7.21 (t, *J* =

7.5 Hz, 3H). **$^{13}C\{^{1}H\}$ NMR (101 MHz, d_6-DMSO) δ (ppm):** 143.0, 140.7, 140.1, 131.9, 125.9, 123.6, 122.8, 121.2, 120.6, 119.4, 118.9, 111.7, 111.4. **HRMS** (ESI) m/z: **$[M+H]^+$ Calcd for $C_{30}H_{21}N_2$** 574.2278; **Found**: 574.2271.

Synthesis of 4-(9H-carbazol-9-yl)-5-fluorophthalonitrile (CzFPN)

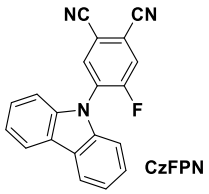

CzFPN

General procedure C

CzFPN was synthesized based on a modified literature protocol.[15] To a 100 mL of flask were added 4,5-difluorophthalonitrile (820 mg, 5.5 mmol, 1.1 equiv.) and sodium hydride (300 mg, 6 mmol, 1.2 equiv.), and the flask was degassed by three cycles of vacuum-nitrogen purging. Carbazole (800 mg, 5 mmol, 1 equiv.) was dissolved in 20 mL of THF and added dropwise into the flask under ice-water bath. After bubbling ceased, the mixture was warmed to room temperature and stirred for 6 h. Afterwards, 1 mL of water was injected to quench the reaction. The mixture was washed with water and extracted with DCM three times (50 mL×3). The organic solvent was removed under reduced pressure and the crude product was purified by column chromatography. DCM/Hexane=1/3 was used as eluent to obtain **CzFPN** as light green solid.

Yield: 80%. **R_f**: 0.55 (50% DCM/Hexane). **Mp:** 225 °C. **^{1}H NMR (400 MHz, $CDCl_3$) δ (ppm):** 8.23 – 8.08 (m, 3H), 7.87 (d, J = 9.0 Hz, 1H), 7.51 (dd, J = 8.3 Hz, 1.3 Hz, 2H), 7.41 (dd, J = 7.5, 1.0 Hz, 2H), 7.28 – 7.18 (m, 2H). **$^{13}C\{^{1}H\}$ NMR (101 MHz, $CDCl_3$) δ (ppm):** 160.7, 158.0,

139.4, 134.6, 131.6, 126.8, 124.5, 123.6, 123.3, 122.0, 120.8, 115.8, 114.0, 113.6. **HRMS** (ESI) m/z: **[M+H]$^+$ Calcd for $C_{20}H_{11}FN_3$** 329.1197; **Found**: 329.1201.

Synthesis of 5,5'-(1,4-phenylenebis(9H-carbazole-3,9-diyl))bis(4-(9H-carbazol-9-yl) phthalonitrile) (*p*-di2CzPN)

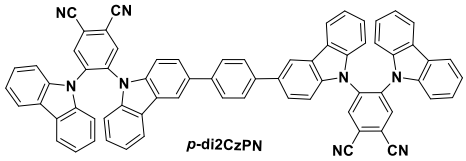

p-di2CzPN

***p*-di2CzPN** was synthesized as **General procedure C**, DCM/Hexane=1/1 was used as eluent and recrystallized in DCM/methanol (1/10) to obtained ***p*-di2CzPN** as yellow solid.

Yield: 50%. **R_f** = 0.40 (60% DCM/Hexane). **Mp:** 278-283 °C. **^{1}H NMR (400 MHz, $CDCl_3$) δ (ppm):** 8.35 (d, *J* = 2.1 Hz, 4H), 8.05 (d, *J* = 1.7 Hz, 2H), 7.92 – 7.79 (m, 6H), 7.60 (s,4H), 7.35 (dd, *J* = 8.6, 1.8 Hz, 2H), 7.23 – 7.07 (m, 20H). **^{13}C{^{1}H} NMR (101 MHz, $CDCl_3$) δ (ppm):** 139.6, 138.8, 138.4, 138.3, 137.8, 135.5, 135.4, 134.4, 127.4, 127.3, 126.5, 126.3, 125.4, 124.9, 124.4, 121.9, 121.7, 120.5, 118.6, 114.8, 114.5, 109.4, 109.2, 109.0. **HRMS** (ESI) m/z: **[M+NH_4]$^+$ Calcd for $C_{70}H_{42}N_9$** 1008.3558; **Found**: 1008.3558. **Elemental analysis: Calcd for $C_{70}H_{38}N_8$**: C, 84.83; H, 3.86; N, 11.31. Found: C, 84.95; H, 3.92; N, 11.20. **HPLC:** 15% H_2O/MeCN, 1.0 mL min^{-1}, 300 nm; tr (99.6 %) = 8.6 min.

Synthesis of 5,5'-(1,3-phenylenebis(9H-carbazole-3,9-diyl))bis(4-(9H-carbazol-9-yl) phthalonitrile) (*m*-di2CzPN)

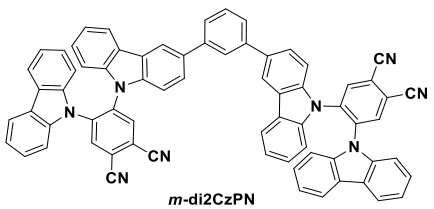

m-di2CzPN

***m*-di2CzPN** was synthesized as **General procedure C** and obtained as yellow solid.

Yield: 60%. $\mathbf{R_f}$: 0.41 (50% DCM/Hexane). **Mp:** 270-276 ºC. **^{1}H NMR (400 MHz, $CDCl_3$) δ (ppm):** 8.37 (d, *J* = 3.6 Hz, 4H), 8.08 (s, 2H), 7.90 (d, *J* = 7.3 Hz, 2H), 7.84 (dd, *J* = 7.4 Hz, 3.5 Hz, 4H), 7.74 (s, 1H), 7.52 (d, *J* = 1.8 Hz, 3H), 7.37 (dd, *J* = 8.5 Hz, 1.7 Hz, 2H), 7.24 – 7.07 (m, 20H). **^{13}C{^{1}H} NMR (101 MHz, $CDCl_3$) δ (ppm):** 141.7, 138.8, 138.5, 138.4, 138.3, 138.3, 137.8, 135.6, 135.4, 135.0, 129.3, 126.6, 126.3, 126.3, 125.8, 125.6, 124. 9, 124.4, 124.3, 121.9, 121.7, 120.5, 119.0, 114.8, 114.8, 114.5, 109.4, 109.2, 109.0, 109.0. **HRMS** (ESI) m/z: **$[M+H]^+$ Calcd for $C_{70}H_{39}N_8$** 991.3292; Found: 991.3296. **Elemental analysis: Calcd for $C_{70}H_{38}N_8$**: C, 84.83; H, 3.86; N, 11.31. Found: C, 84.72; H, 3.92; N, 11.19. **HPLC:** 15% H_2O/MeCN, 1.0 mL min^{-1}, 300 nm; tr (99.2 %) = 7.9 min.

Synthesis of 5,5',5''-(benzene-1,3,5-triyltris(9H-carbazole-3,9-diyl))tris(4-(9H-carbazol-9-yl) phthalonitrile) (1,3,5-tri2CzPN)

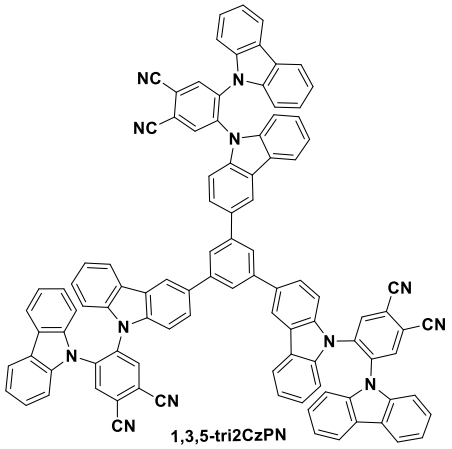

1,3,5-tri2CzPN was synthesized as **General procedure C** and obtained as yellow solid.

Yield: 55%. $\mathbf{R_f}$: 0.38 (50% DCM/Hexane). **Mp:** 310-315 ºC. **^{1}H NMR (400 MHz, $CDCl_3$) δ (ppm):** 8.38 (d, *J* = 4.0 Hz, 6H), 8.13 (d, *J* = 1.7 Hz, 3H), 7.97 – 7.90 (m, 3H), 7.87 - 7.82 (m, 6H), 7.69 (s, 3H), 7.43 (dd, *J* = 8.5 Hz, 1.5 Hz, 3H), 7.21 – 7.08 (m, 30H). **^{13}C{^{1}H} NMR (101**

MHz, $CDCl_3$) δ (ppm): 142.3, 138.9, 138.4, 138.0, 135.6, 135.4, 134.8, 126.6, 126.4, 125.7, 124.9, 124.8, 124.4, 124.3, 121.9, 121.7, 120.6, 119.0, 114.9, 114.5, 109.5, 109.3, 109.1. **HRMS** (ESI) m/z: **$[M+H]^+$ Calcd for $C_{102}H_{55}N_{12}$** 1447.4667; **Found**: 1447.4677. **Elemental analysis: Calcd for $C_{102}H_{54}N_{12}$**: C, 84.63; H, 3.76; N, 11.61. Found: C, 84.59; H, 3.65; N, 11.72. **HPLC:** 10% H_2O/MeCN, 1.0 mL min^{-1}, 300 nm; tr (99.6 %) = 5.6 min.

Supporting Information

Compound characterization, computational details, instrumental details, thermal stability, device fabrication details are available in Supporting Information.

Acknowledgements

D.C thanks the China Scholarship Council (201603780001). P. R acknowledges support from a Marie Skłodowska-Curie Individual Fellowship (No. 749557). D. S. acknowledges support from the Marie Skłodowska-Curie Individual Fellowship (No. 838009). We acknowledge support from the Engineering and Physical Sciences Research Council of the United Kingdom (grant EP/P010482/1), from the International Collaborative Research Program of Institute for Chemical Research, Kyoto University (Nos. 2020-37 and 2021-37), and from JSPS KAKENHI Grant Number JP20H05840 (Grant-in-Aid for Transformative Research Areas, “Dynamic Exciton”).

References.

(1) Tang, C. W.; Vanslyke, S. A. Organic Electroluminescent Diodes. *Appl. Phys. Lett.* **1987**, *51* (12), 913–915. https://doi.org/10.1063/1.98799.

(2) Wong, M. Y.; Zysman-colman, E. Purely Organic Thermally Activated Delayed Fluorescence Materials for Organic Light-Emitting Diodes. *Adv. Mater.* **2017**, *29*, 1605444. https://doi.org/10.1002/adma.201605444.

(3) Song, J.; Lee, H.; Jeong, E. G.; Choi, K. C.; Yoo, S. Organic Light-Emitting Diodes: Pushing Toward the Limits and Beyond. *Adv. Mater.* **2020**, *32* (35), 1907539. https://doi.org/10.1002/adma.201907539.

(4) Hong, G.; Gan, X.; Leonhardt, C.; Zhang, Z.; Seibert, J.; Busch, J. M.; Bräse, S. A Brief History of OLEDs—Emitter Development and Industry Milestones. *Adv. Mater.* **2021**, *33* (9), 2005630. https://doi.org/10.1002/adma.202005630.

(5) Kido, J.; Kimura, M.; Nagai, K. Multilayer White Light-Emitting Organic Electroluminescent Device. *Science* **1995**, *267* (5202), 1332–1334. https://doi.org/10.1126/science.267.5202.1332.

(6) Multilayer, O.; Emitting, L. Electroluminescence of 1,3,4-Oxadiazole and Triphenylamine-Containing Molecules as an Emitter in Organic Multilayer Light Emitting Diodes. *Chem. Mater.* **1997**, *4756* (18), 1077–1085.

(7) Lee, J.; Chen, H. F.; Batagoda, T.; Coburn, C.; Djurovich, P. I.; Thompson, M. E.; Forrest, S. R. Deep Blue Phosphorescent Organic Light-Emitting Diodes with Very High Brightness and Efficiency. *Nat. Mater.* **2016**, *15* (1), 92–98. https://doi.org/10.1038/nmat4446.

(8) Kim, D. H.; D'Aléo, A.; Chen, X. K.; Sandanayaka, A. D. S.; Yao, D.; Zhao, L.; Komino, T.; Zaborova, E.; Canard, G.; Tsuchiya, Y.; Choi, E.; Wu, J. W.; Fages, F.; Brédas, J. L.; Ribierre, J. C.; Adachi, C. High-Efficiency Electroluminescence and Amplified Spontaneous Emission from a Thermally Activated Delayed Fluorescent near-Infrared Emitter. *Nat. Photonics* **2018**, *12* (2), 98–104. https://doi.org/10.1038/s41566-017-0087-y.

(9) Segal, M.; Baldo, A.; Holmes, J.; Forrest, R.; Soos, G. Excitonic Singlet-Triplet Ratios in Molecular and Polymeric Organic Materials. *Phys. Rev. B - Condens. Matter Mater. Phys.* **2003**, *68* (7), 075211. https://doi.org/10.1103/PhysRevB.68.075211.

(10) Baldo, M. A.; O'Brien, D. F.; You, Y.; Shoustikov, A.; Sibley, S.; Thompson, M. E.; Forrest, S. R. Highly Efficient Phosphorescent Emission from Organic Electroluminescent Devices. *Nature* **1998**, *395* (6698), 151–154. https://doi.org/10.1038/25954.

(11) Ma, Y.; Che, C. M.; Chao, H. Y.; Zhou, X.; Chan, W. H.; Shen, J. High Luminescence Gold(I) and Copper(I) Complexes with a Triplet Excited State for Use in Light-Emitting Diodes. *Adv. Mater.* **1999**, *11* (10), 852–857. https://doi.org/10.1002/(SICI)1521-4095(199907)11:10<852::AID-ADMA852>3.0.CO;2-R.

(12) Yook, K. S.; Lee, J. Y. Organic Materials for Deep Blue Phosphorescent Organic Light-Emitting Diodes. *Adv. Mater.* **2012**, *24* (24), 3169–3190. https://doi.org/10.1002/adma.201200627.

(13) Hudson, Z. M.; Sun, C.; Helander, M. G.; Chang, Y. L.; Lu, Z. H.; Wang, S. Highly Efficient Blue Phosphorescence from Triarylboron-Functionalized Platinum(II) Complexes of N-Heterocyclic Carbenes. *J. Am. Chem. Soc.* **2012**, *134* (34), 13930–13933. https://doi.org/10.1021/ja3048656.

(14) Endo, A.; Sato, K.; Yoshimura, K.; Kai, T.; Kawada, A.; Miyazaki, H.; Adachi, C. Efficient Up-Conversion of Triplet Excitons into a Singlet State and Its Application for Organic Light Emitting Diodes. *Appl. Phys. Lett.* **2011**, *98* (8), 083302. https://doi.org/10.1063/1.3558906.

(15) Uoyama, H.; Goushi, K.; Shizu, K.; Nomura, H.; Adachi, C. Highly Efficient Organic Light-Emitting Diodes from Delayed Fluorescence. *Nature* **2012**, *492* (7428), 234–238.

(16) Dias, F. B.; Bourdakos, K. N.; Jankus, V.; Moss, K. C.; Kamtekar, K. T.; Bhalla, V.; Santos, J.; Bryce, M. R.; Monkman, A. P. Triplet Harvesting with 100% Efficiency by Way of Thermally Activated Delayed Fluorescence in Charge Transfer OLED Emitters. *Adv. Mater.* **2013**, *25* (27), 3707–3714. https://doi.org/10.1002/adma.201300753.

(17) Nakanotani, H.; Higuchi, T.; Furukawa, T.; Masui, K.; Morimoto, K.; Numata, M.; Tanaka, H.; Sagara, Y.; Yasuda, T.; Adachi, C. High-Efficiency Organic Light-Emitting Diodes with Fluorescent Emitters. *Nat. Commun.* **2014**, *5*, 4016. https://doi.org/10.1038/ncomms5016.

(18) Chen, D. Y.; Liu, W.; Zheng, C. J.; Wang, K.; Li, F.; Tao, S. L.; Ou, X. M.; Zhang, X. H. Isomeric Thermally Activated Delayed Fluorescence Emitters for Color Purity-Improved Emission in Organic Light-Emitting Devices. *ACS Appl. Mater. Interfaces* **2016**, *8* (26), 16791–16798. https://doi.org/10.1021/acsami.6b03954.

(19) Dos Santos, P. L.; Chen, D.; Rajamalli, P.; Matulaitis, T.; Cordes, D. B.; Slawin, A. M. Z.; Jacquemin, D.; Zysman-Colman, E.; Samuel, I. D. W. Use of Pyrimidine and Pyrazine Bridges as a Design Strategy to Improve the Performance of Thermally Activated Delayed Fluorescence Organic Light Emitting Diodes. *ACS Appl. Mater. Interfaces* **2019**, *11* (48), 45171–45179. https://doi.org/10.1021/acsami.9b16952.

(20) Zhang, Z.; Crovini, E.; dos Santos, P. L.; Naqvi, B. A.; Cordes, D. B.; Slawin, A. M. Z.; Sahay, P.; Brütting, W.; Samuel, I. D. W.; Bräse, S.; Zysman-Colman, E. Efficient Sky-Blue Organic Light-Emitting Diodes Using a Highly Horizontally Oriented Thermally Activated Delayed Fluorescence Emitter. *Adv. Opt. Mater.* **2020**, *8* (23), 2001354. https://doi.org/10.1002/adom.202001354.

(21) Kaji, H.; Suzuki, H.; Fukushima, T.; Shizu, K.; Suzuki, K.; Kubo, S.; Komino, T.; Oiwa, H.; Suzuki, F.; Wakamiya, A.; Murata, Y.; Adachi, C. Purely Organic Electroluminescent Material Realizing 100% Conversion from Electricity to Light. *Nat. Commun.* **2015**, *6*, 9476. https://doi.org/10.1038/ncomms9476.

(22) Samanta, P. K.; Kim, D.; Coropceanu, V.; Brédas, J. L. Up-Conversion Intersystem Crossing Rates in Organic Emitters for Thermally Activated

Delayed Fluorescence: Impact of the Nature of Singlet vs Triplet Excited States. *J. Am. Chem. Soc.* **2017**, *139* (11), 4042–4051. https://doi.org/10.1021/jacs.6b12124.

(23) Tsujimoto, H.; Ha, D.-G.; Markopoulos, G.; Chae, H. S.; Baldo, M. A.; Swager, T. M. Thermally Activated Delayed Fluorescence and Aggregation Induced Emission with Through-Space Charge Transfer. *J. Am. Chem. Soc.* **2017**, *139* (13), 4894–4900. https://doi.org/10.1021/jacs.7b00873.

(24) Wang, K.; Zheng, C. J.; Liu, W.; Liang, K.; Shi, Y. Z.; Tao, S. L.; Lee, C. S.; Ou, X. M.; Zhang, X. H. Avoiding Energy Loss on TADF Emitters: Controlling the Dual Conformations of D–A Structure Molecules Based on the Pseudoplanar Segments. *Adv. Mater.* **2017**, *29* (47), 1701476. https://doi.org/10.1002/adma.201701476.

(25) Rajamalli, P.; Senthilkumar, N.; Huang, P. Y.; Ren-Wu, C. C.; Lin, H. W.; Cheng, C. H. New Molecular Design Concurrently Providing Superior Pure Blue, Thermally Activated Delayed Fluorescence and Optical Out-Coupling Efficiencies. *J. Am. Chem. Soc.* **2017**, *139* (32), 10948–10951. https://doi.org/10.1021/jacs.7b03848.

(26) Hall, D.; Suresh, S. M.; dos Santos, P. L.; Duda, E.; Bagnich, S.; Pershin, A.; Rajamalli, P.; Cordes, D. B.; Slawin, A. M. Z.; Beljonne, D.; Köhler, A.; Samuel, I. D. W.; Olivier, Y.; Zysman-Colman, E. Improving Processability and Efficiency of Resonant TADF Emitters: A Design Strategy. *Adv. Opt. Mater.* **2020**, *8*, 1901627. https://doi.org/10.1002/adom.201901627.

(27) Cui, L.; Gillett, A. J.; Zhang, S.; Ye, H.; Liu, Y.; Chen, X.; Lin, Z.; Evans, E. W.; Myers, W. K.; Ronson, T. K.; Nakanotani, H.; Reineke, S.; Bredas, J.; Adachi, C.; Friend, R. H. Fast Spin-Flip Enables Efficient and Stable Organic Electroluminescence from Charge-Transfer States. *Nat. Photon.* **2020**, *14*, 636–642.

(28) Hilborn, R. C. Einstein Coefficients, Cross Sections, f Values, Dipole Moments, and All That . *Am. J. Phys.* **1982**, *50* (11), 982–986. https://doi.org/10.1119/1.12937.

(29) Cho, Y. J.; Jeon, S. K.; Chin, B. D.; Yu, E.; Lee, J. Y. The Design of Dual Emitting Cores for Green Thermally Activated Delayed Fluorescent Materials. *Angew. Chemie Int. Ed.* **2015**, *54* (17), 5201–5204. https://doi.org/10.1002/anie.201412107.

(30) Kim, M.; Jeon, S. K.; Hwang, S. H.; Lee, S. S.; Yu, E.; Lee, J. Y. Highly Efficient and Color Tunable Thermally Activated Delayed Fluorescent Emitters Using a "Twin Emitter" Molecular Design. *Chem. Commun.* **2016**, *52* (2), 339–342. https://doi.org/10.1039/c5cc07999c.

(31) Cho, Y. J.; Jeon, S. K.; Lee, S. S.; Yu, E.; Lee, J. Y. Donor Interlocked Molecular Design for Fluorescence-like Narrow Emission in Deep Blue Thermally Activated Delayed Fluorescent Emitters. *Chem. Mater.* **2016**, *28* (15), 5400–5405. https://doi.org/10.1021/acs.chemmater.6b01484.

(32) Park, H.-J.; Han, S. H.; Lee, J. Y. A Directly Coupled Dual Emitting Core Based Molecular Design of Thermally Activated Delayed Fluorescent Emitters. *J.*

Mater. Chem. C **2017**, *5*, 12143–12150. https://doi.org/10.1039/C7TC03133E.

(33) Cha, J. R.; Lee, C. W.; Lee, J. Y.; Gong, M. S. Design of Ortho-Linkage Carbazole-Triazine Structure for High-Efficiency Blue Thermally Activated Delayed Fluorescent Emitters. *Dye. Pigment.* **2016**, *134*, 562–568. https://doi.org/10.1016/j.dyepig.2016.08.023.

(34) Wei, D.; Ni, F.; Wu, Z.; Zhu, Z.; Zou, Y.; Zheng, K.; Chen, Z.; Ma, D.; Yang, C. Designing Dual Emitting Cores for Highly Efficient Thermally Activated Delayed Fluorescent Emitters. *J. Mater. Chem. C* **2018**, *6* (43), 11615–11621. https://doi.org/10.1039/c8tc02849d.

(35) Park, S. Y.; Choi, S.; Park, G. E.; Kim, H. J.; Lee, C.; Moon, J. S.; Kim, S. W.; Park, S.; Kwon, J. H.; Cho, M. J.; Choi, D. H. Unconventional Three-Armed Luminogens Exhibiting Both Aggregation-Induced Emission and Thermally Activated Delayed Fluorescence Resulting in High-Performing Solution-Processed OLEDs. *ACS Appl. Mater. Interfaces* **2018**, *10*, 14966–14977. https://doi.org/10.1021/acsami.7b19681.

(36) Chen, D.; Kusakabe, Y.; Ren, Y.; Sun, D.; Rajamalli, P.; Wada, Y.; Suzuki, K.; Kaji, H.; Zysman-Colman, E. Multichromophore Molecular Design for Efficient Thermally Activated Delayed Fluorescence Emitters with Near-Unity Photoluminescence Quantum Yields. **2021**. https://doi.org/https://doi.org/10.26434/chemrvix.14560860.v1.

(37) Zysman-Colman, E.; Arias, K.; Siegel, J. S. Synthesis of Arylbromides from Arenes and Nbromosuccinimide Bromosuccinimide (NBS) in Acetonitrile - A Convenient Method for Aromatic Bromination. *Can. J. Chem.* **2009**, *87* (2), 440–447. https://doi.org/10.1139/V08-176.

(38) Wong, M. Y.; La-Placa, M.-G.; Pertegas, A.; Bolink, H. J.; Zysman-Colman, E. Deep-Blue Thermally Activated Delayed Fluorescence (TADF) Emitters for Light-Emitting Electrochemical Cells (LEECs). *J. Mater. Chem. C* **2017**, *5* (7), 1699–1705. https://doi.org/10.1039/C6TC04821H.

(39) Chen, B.; Ding, J.; Wang, L.; Jing, X.; Wang, F. A Solution-Processable Phosphonate Functionalized Deep-Blue Fluorescent Emitter for Efficient Single-Layer Small Molecule Organic Light-Emitting Diodes. *Chem. Commun.* **2012**, *48* (71), 8970–8972. https://doi.org/10.1039/c2cc34712a.

(40) Ishiyama, T.; Murata, M.; Miyaura, N. Palladium(0)-Catalyzed Cross-Coupling Reaction of Alkoxydiboron with Haloarenes: A Direct Procedure for Arylboronic Esters. *J. Org. Chem.* **1995**, *60* (23), 7508–7510. https://doi.org/10.1021/jo00128a024.

(41) Pople, J. A.; Binkley, J. S.; Seeger, R. Theoretical Models Incorporating Electron Correlation. *Int. J. Quantum Chem.* **1976**, *10*, 1–19. https://doi.org/10.1002/qua.560100802.

(42) Adamo, C.; Barone, V. Toward Reliable Density Functional Methods without Adjustable Parameters: The PBE0 Model. *J. Chem. Phys.* **1999**, *110* (13), 6158–6170. https://doi.org/10.1063/1.478522.

(43) Moral, M.; Muccioli, L.; Son, W. J.; Olivier, Y.; Sancho-Garcia, J. C. Theoretical Rationalization of the Singlet-Triplet Gap in Oleds Materials: Impact of Charge-

Transfer Character. *J. Chem. Theory Comput.* **2015**, *11* (1), 168–177. https://doi.org/10.1021/ct500957s.

(44) Pavlishchuk, V. V.; Addison, A. W. Conversion Constants for Redox Potentials Measured versus Different Reference Electrodes in Acetonitrile Solutions at 25°C. *Inorganica Chim. Acta* **2000**, *298*, 97–102. https://doi.org/10.1016/S0020-1693(99)00407-7.

(45) Wong, M. Y.; Krotkus, S.; Copley, G.; Li, W.; Murawski, C.; Hall, D.; Hedley, G. J.; Jaricot, M.; Cordes, D. B.; Slawin, A. M. Z.; Olivier, Y.; Beljonne, D.; Muccioli, L.; Moral, M.; Sancho-Garcia, J.-C.; Gather, M. C.; Samuel, I. D. W.; Zysman-Colman, E. Deep-Blue Oxadiazole-Containing Thermally Activated Delayed Fluorescence Emitters for Organic Light-Emitting Diodes. *ACS Appl. Mater. Interfaces* **2018**, *10* (39), 33360–33372. https://doi.org/10.1021/acsami.8b11136.

(46) Wang, X.; Yan, Q.; Chu, P.; Luo, Y.; Zhang, Z.; Wu, S.; Wang, L.; Zhang, Q. Analysis on Fluorescence of Dual Excitable Eu(TTA)3DPBT in Toluene Solution and PMMA. *J. Lumin.* **2011**, *131* (8), 1719–1723. https://doi.org/10.1016/j.jlumin.2011.03.061.

(47) dos Santos, P. L.; Ward, J. S.; Congrave, D. G.; Batsanov, A. S.; Stacey, J. E.; Penfold, T. J.; Monkman, A. P.; Bryce, M. R. Triazatruxene: A Rigid Central Donor Unit for a D-A3 Thermally Activated Delayed Fluorescence Material Exhibiting Sub-Microsecond Reverse Intersystem Crossing and Unity Quantum Yield via Multiple Singlet-Triplet State Pairs. *Adv. Sci.* **2018**, *5*, 1700989. https://doi.org/10.1002/advs.201700989.

TOC